Available online at www.sciencedirect.com
ScienceDirect
Journal of Fluorine Chemistry 128 (2007) 438–447
JOURNAL OF FLUORINE CHEMISTRY
www.elsevier.com/locate/fluor

Review

Preparation and properties of rare-earth containing oxide fluoride glasses

Susumu Yonezawa [a,*], Shiori Nishibu [a], Marc Leblanc [b], Masayuki Takashima [a]

[a] *Graduate School of Engineering, University of Fukui, Bunkyo 3-9-1, Fukui 910-8507, Japan*
[b] *Laboratoire des Oxydes et Fluorures, UMR CNRS 6010, Faculté des Sciences et Techniques, Université du Maine, Avenue Olivier Messiaen, 72085 Le Mans Cedex 09, France*

Received 31 August 2006; received in revised form 28 November 2006; accepted 3 December 2006
Available online 6 December 2006

Abstract

The preparation of the rare earth containing oxide fluoride glasses LnF_3 (Ln; Y through Lu)–BaF_2–AlF_3–GeO_2 in which the nominal content of LnF_3 reached 60 mol% in maximum and their basic properties such as density, refractive index and glass transition temperature were investigated and summarized in detail. Especially, in order to discuss the local structure around the rare earth ion in the glass, the Judd–Ofelt analysis (discussion with Ω parameters) of the HoF_3–BaF_2–AlF_3–GeO_2 glasses was carried out. The unique fluorescent behavior and the magnetic properties of LnF_3–BaF_2–AlF_3–GeO_2 glasses (Ln = Tb and/or Sm) were also studied.

Keywords: Oxide fluoride glass; Preparation; Rare earth; Optical property; Magnetic property

Contents

1. Introduction

Our previous works have revealed that the solid electrolyte written by $Ln_2Ln'_2O_3F_6$ where Ln and Ln′ are different rare earths showed higher conductivity than that of YSZ; it has usefully stable for an oxide ion-conducting solid electrode under 700 °C [1]. Their conductivity performance depends on the combination of rare earth elements. The Nd–Sm system and Nd–Eu system showed the highest conductivity among all combinations. During the preparation process of the material of the solid electrolyte, a glass was obtained by chance. From quantitative analysis using EPMA, this glass evidently contained all starting elements (O, F and two species of rare earth elements). In addition, Si and Al, which were not contained in starting materials, were detected in the glass. The binary rare earth oxide fluoride solid electrode was prepared using a solid state reaction between a rare earth oxide (Ln_2O_3) and a rare earth fluoride ($Ln'F_3$) at a temperature higher than 1000 °C. During the mixing process, an agate ball mill was used to mix the starting materials. During calcination, the mixture was heated to over 1000 °C after it was packed into an alumina tube. The Si and Al in the glass had to be supplied from these

* Corresponding author.
E-mail address: yonezawa@matse.fukui-u.ac.jp (S. Yonezawa).

0022-1139/$ – see front matter © 2006 Elsevier B.V. All rights reserved.
doi:10.1016/j.jfluchem.2006.12.002

materials as glass network formers. This glass was shown to contain more than 70 wt% of rare earth elements from results of the analysis using EPMA (FP method). The obtained glass was a new oxide fluoride glass containing a large amount of rare earth element. Several reports have described preparation of glasses containing rare earth elements for use as optical or magneto-optical materials [2–6]. Every rare earth element has unique optical properties because of its arrangement of electrons in the 4f orbital. It is important to find matrices in which these rare earth elements can be doped and can exhibit their performance to develop new optical and magnetic materials. Oxide fluoride glasses contain two different anions that have different valence electrons and different degrees of polarization. It is interesting to compare properties of the oxide fluoride glass with those of the oxide or fluoride glass. No reports have addressed a glass that can contain rare earth fluoride with such a high content. The properties of oxide fluoride glasses have not been summarized systematically yet, as they have been for oxide glasses or fluoride glasses. It is very interesting to study the preparation processes and characteristics of these glasses to develop new functional materials. In this paper, several recent results about rare-earth containing oxide fluoride glasses are reported.

2. Results and discussion

2.1. Preparation and basic characteristics of oxide fluoride glasses containing LnF_3

This section describes the preparation process and basic characterization of oxide fluoride glasses containing NdF_3 (light rare earth), TbF_3 (middle rare earth), and HoF_3 (heavy rare earth). Based on those results, preparation methods could be extended to other rare earth elements in the lanthanide series. Properties of those glasses were compared and summarized.

2.1.1. Preparation of oxide fluoride glasses containing LnF_3

The glass in the NdF_3–SiO_2–Al_2O_3 system has been obtained once. However, the reproducibility was not confirmed. After analyzing the glass in detail, it seemed that AlF_3 could be contained in the product in NdF_3–SiO_2–Al_2O_3 system. It means that some part of NdF_3 has been hydrolyzed to form HF and this HF has reacted with Al_2O_3 to form AlF_3. Controlling the content of AlF_3 seems to be important factor to prepare the oxide fluoride glass reproducibly. But the higher temperature for melting the sample causes large variation of the AlF_3 content in the product because AlF_3 sublimes at a temperature higher than 1000 °C remarkably. In addition, rare earth trifluorides easily undergoes pyro-hydrolysis to form their oxides over 1000 °C [7]. As the network forming oxide GeO_2 was chosen because of the lowest melting point among SiO_2 (1730 °C), Al_2O_3 (2045 °C) and GeO_2 (116 °C) in this study. In addition, various fluorides were tested as glass network modifiers and additives to lower the melting point. Consequently, the oxide fluoride glasses containing light rare earth (NdF_3) became to be obtainable in the system of NdF_3–AlF_3–GeO_2 reproducibly. Fig. 1 shows a phase diagram of the

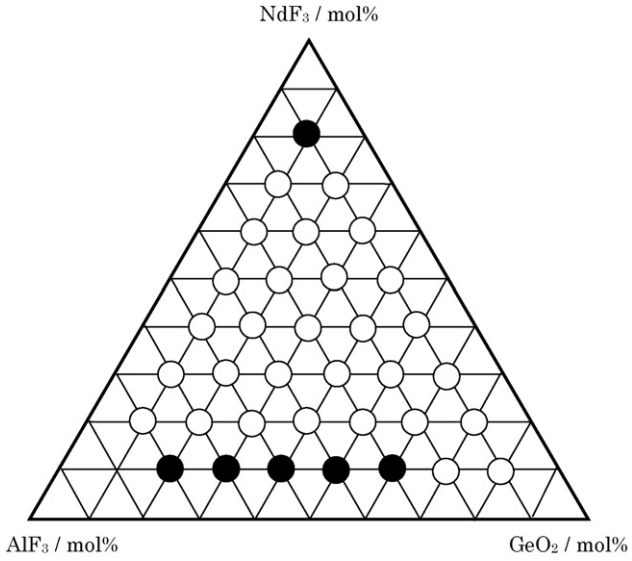

Fig. 1. Phase diagram of NdF_3–AlF_3–GeO_2 system shown by nominal composition. Closed and open circles, respectively, indicate crystal and glass phases.

NdF_3–AlF_3–GeO_2 system. It had a wide glass formation composition area. The glass was capable of containing 70 mol% NdF_3 as a nominal composition. These glasses containing NdF_3 showed the alexandrite effect. That is, the color of obtained glass showed red-violet under continuous light like sunlight and blue-violet under discontinuous light like fluorescent light. Quantitative analyses by ZAF method using EPMA showed clearly that the obtained glass was incapable of maintaining its nominal composition. Fig. 2 shows the cationic composition in the products of NdF_3–AlF_3–GeO_2 system measured by using EPMA. Contents of Al especially tended to decrease from the starting ratio. The Al contents in the glass never became greater than 34 mol%, even if the starting material contained more than 34 mol% Al. The Nd content reached 63 mol% as the maximum value. Glasses with the rare earth content more than 30 mol% have not been reported yet. These oxide fluoride glasses with a high content of rare earths are anticipated as new functional materials.

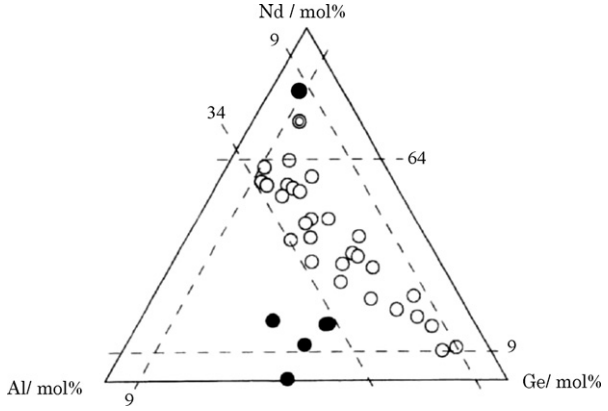

Fig. 2. Cationic composition in the glass of NdF_3–AlF_3–GeO_2 system measured by EPMA. Closed and open circles, respectively, indicate crystal and glass phases.

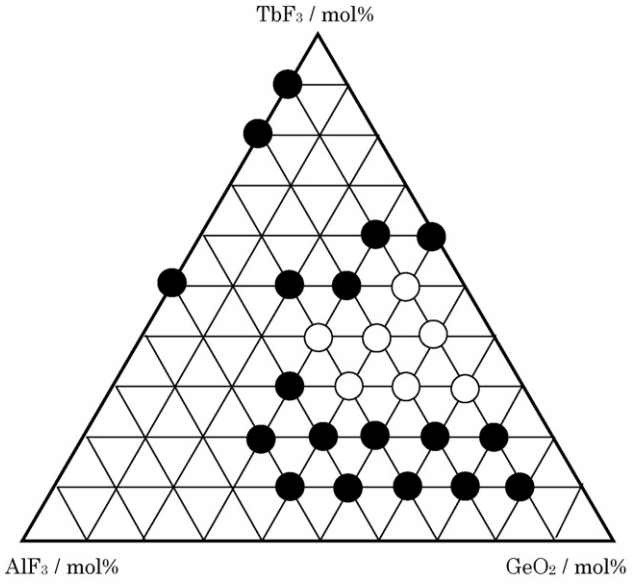

Fig. 3. Phase diagram of TbF_3–AlF_3–GeO_2 system shown by nominal composition. Closed and open circles, respectively, indicate crystal and glass phases.

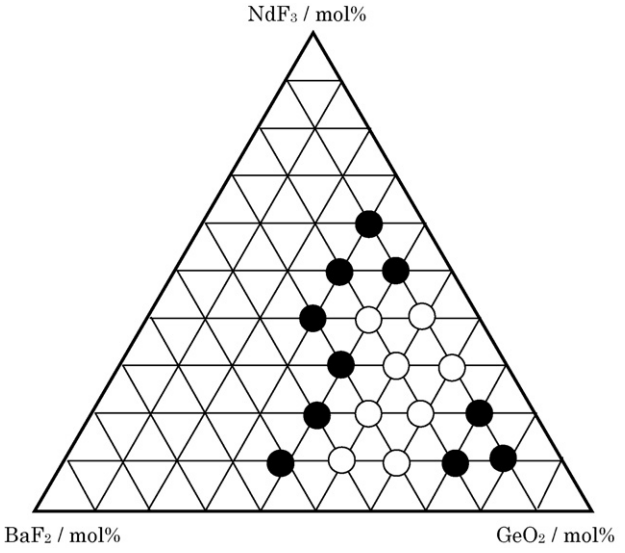

Fig. 5. Phase diagram of NdF_3–BaF_2–GeO_2 system shown by nominal composition. Closed and open circles, respectively, indicate crystal and glass phases.

Fig. 3 shows a phase diagram of TbF_3–AlF_3–GeO_2. The maximum TbF_3 content was 50 mol% in the glass. The glass formation composition area as shown in Fig. 3 is smaller than that of the TbF_3–AlF_3–GeO_2 glasses shown in Fig. 1. It has been reported that rare earth trifluorides hydrolyzed at a temperature higher than 700 °C [7,8], the melting temperature should be lower to avoid composition changes during high temperature processing. As shown in Fig. 4, the results of quantitative analyses obtained by EPMA measurement of TbF_3–AlF_3–GeO_2 glasses showed that the cationic compositions in the glass deviated from that of the starting ratio. Furthermore, the composition change in the glass increased with increasing AlF_3 content. This system did not contain glass with 50 mol% TbF_3, even if the glass was obtained from a starting mixture containing 50 mol% TbF_3. The amount of AlF_3 must be optimized to realize good reproducibility, because the excess of AlF_3 drastically changes the glass composition from the starting ratio.

The BaF_2 was added to starting materials instead of AlF_3 because BaF_2 hardly not only sublime but hydrolyze at melting temperatures of 1200 °C. Fig. 5 presents a phase diagram of the NdF_3–BaF_2–GeO_2 system. This system had a large glass formation composition area and the content of NdF_3 in the glass reached 40 mol% as a nominal composition. Fig. 6 shows the cationic composition in the glasses of NdF_3–BaF_2–GeO_2 system resulted from quantitative analyses by using EPMA.

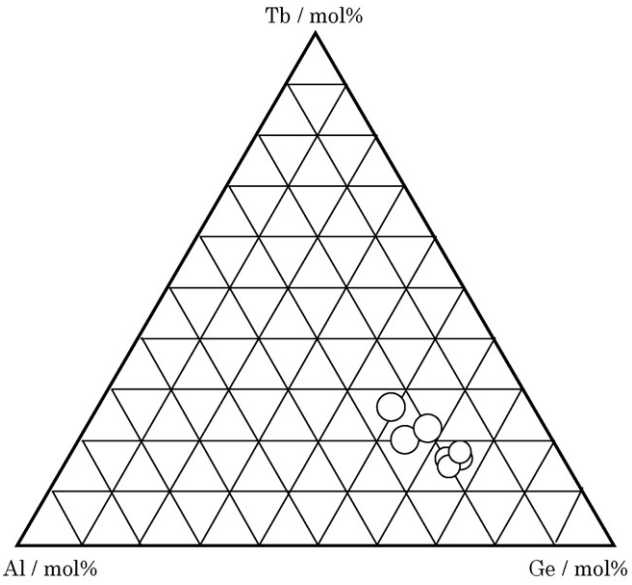

Fig. 4. Cationic composition in the glass of TbF_3–AlF_3–GeO_2 system glasses measured by EPMA.

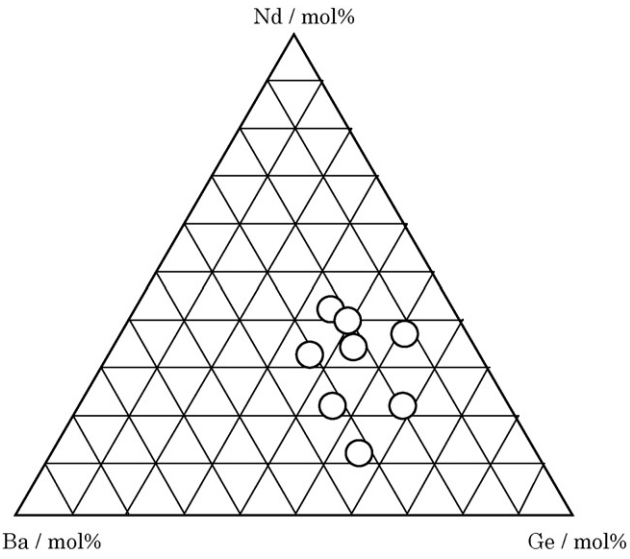

Fig. 6. Cationic composition in the glass of NdF_3–BaF_2–GeO_2 system measured by EPMA.

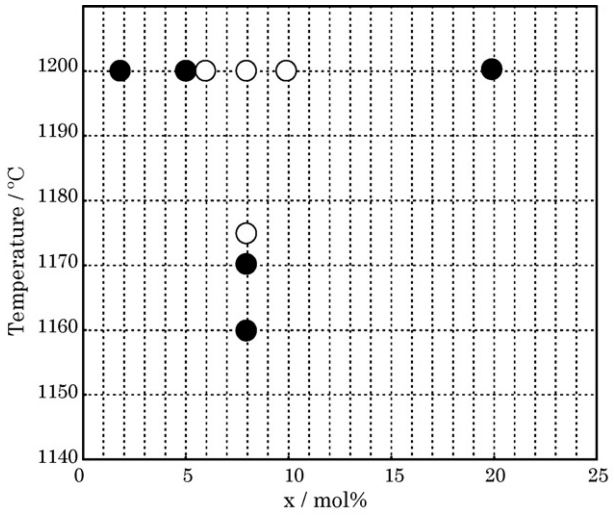

Fig. 7. Classification of the products for $10HoF_3$–$(30-x)BaF_2$ – $xAlF_3$–$60GeO_2$ systems at various melting temperatures. (○) and (●) mean the glass and crystalline phases, respectively.

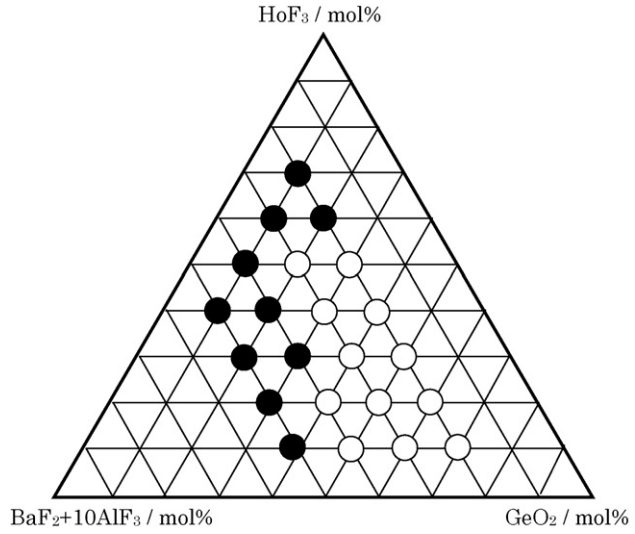

Fig. 8. Phase diagram of HoF_3–BaF_2–$10AlF_3$–GeO_2 shown by nominal composition. The AlF_3 content was fixed at 10 mol%. Closed and open circles, respectively, indicate crystal and glass phases.

The obtained glass in this system maintained the starting cationic compositions rather than the NdF_3–AlF_3–GeO_2 system did. Apparently, the addition of BaF_2 assisted to obtain the oxide fluoride glass reproducibly and assisted to maintain the nominal composition in the glass. Overall, BaF_2 was a better component to prepare the oxide fluoride glass containing NdF_3 than AlF_3 was. Based on results of the glass preparation in the ternary system glass, it was tired to prepare $40LnF_3$–$20BaF_2$–$40GeO_2$ (Ln; La–Nd, Sm–Lu) glasses by melting at 1200 °C for 1.5 h. Only in case of NdF_3, SmF_3, EuF_3, and GdF_3 (middle rare earth fluorides), the glasses were obtained.

Choosing the system containing HoF_3, a glass formation process with heavy rare earth trifluoride was investigated. Several chemicals were tested for use as additive components to obtain oxide fluoride glasses at lower melting temperatures and with lower weight loss during melting. Finally, it has been found that both BaF_2 and AlF_3 are necessary to obtain the glasses containing HoF_3 reproducibly and the accurate controls of their contents are needed. Fig. 7 shows the glass forming condition relative to the quantity of AlF_3 and melting temperature. The oxide fluoride glasses were obtainable reproducibly by adding more than 6 mol% AlF_3; excessive AlF_3 caused a change in glass composition as described above. The AlF_3 content would be better to be maintained at ca. 10 mol% to obtain glass reproducibly without composition change through the melting process. The glass was possible to be prepared at 1175 °C in case of GeO_2 system, whereas about 1300 °C was needed in case of the SiO_2 system.

Fig. 8 shows a phase diagram of the HoF_3–BaF_2–AlF_3–GeO_2 system in which the AlF_3 content was fixed at 10 mol%. This diagram shows that this glass system has a wide composition range for glass formation. An oxide fluoride glass was prepared with maximum content of HoF_3 of 50 mol%. For the $50HoF_3$–$10BaF_2$–$10AlF_3$–$30GeO_2$ glass represented in Fig. 8, the glass network structure or the environment of Ho^{3+} ion shows a different view from that of a $10HoF_3$–$10BaF_2$–$10AlF_3$–$70GeO_2$ glass because its quantity of the glass-forming oxide (GeO_2) is different. Fig. 9 shows results of quantitative analyses of HoF_3–BaF_2–AlF_3–GeO_2 glasses using EPMA (ZAF method). As a result, only slight deviation of the cationic composition in the glass product from the nominal composition of the starting mixture was recognized. Regarding $10HoF_3$–$10BaF_2$–$10AlF_3$–$70GeO_2$ and the $50HoF_3$–$10BaF_2$–$10AlF_3$–$30GeO_2$ glasses, the respective analytical cationic ratios in the product glasses are Ho:Ba:Al:Ge = 6.1:9.0:11.6:73.2 and 41.4:13.6:8.8:36.1. These values approximately agreed with the nominal composition.

Fig. 10 shows the phase diagram of TbF_3–BaF_2–$10AlF_3$–GeO_2. The AlF_3 content was fixed at 10 mol%; the content of BaF_2 was adjusted instead of the excess AlF_3 to avoid a

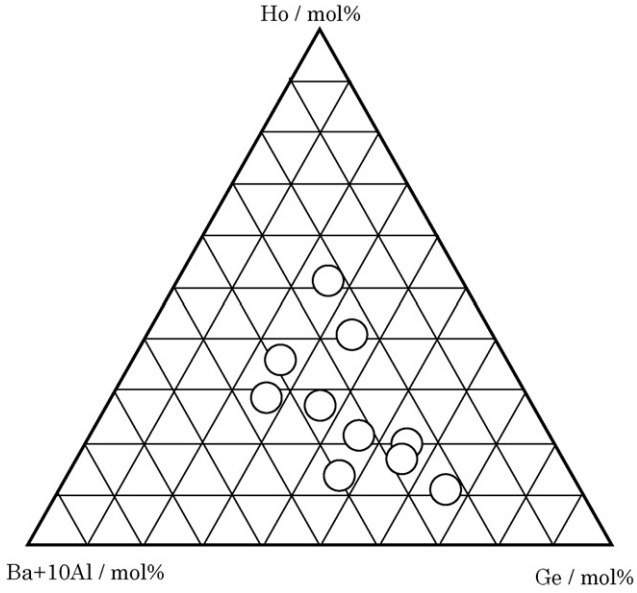

Fig. 9. Cationic composition in the glass of HoF_3–BaF_2–AlF_3–GeO_2 system measured by EPMA.

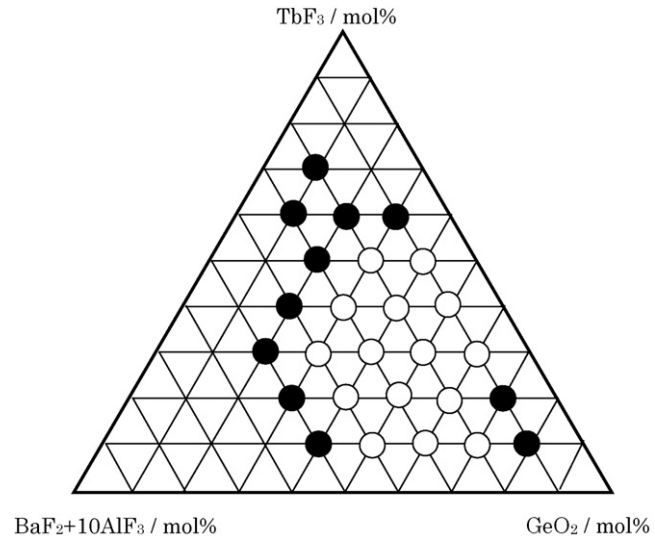

Fig. 10. Phase diagram of TbF_3–BaF_2–$10AlF_3$–GeO_2 shown by nominal composition. The AlF_3 content was fixed at 10 mol%. Closed and open circles, respectively, indicate crystal and glass phases.

composition change through the melting process. Fig. 11 shows the cationic composition of TbF_3–BaF_2–$10AlF_3$–GeO_2 glasses obtained by quantitative analyses with EPMA. The cationic compositions in the glasses were found to be maintained almost as the starting ratio. The maximum content of TbF_3 was 50 mol% as a starting ratio. In this TbF_3–BaF_2–$10AlF_3$–GeO_2 system, glasses with wide variation in terbium contents can be prepared reproducibly. At last, the glasses were obtained in LnF_3–BaF_2–$10AlF_3$–GeO_2 system for Ln = La–Lu (except for Pm) reproducibly.

2.1.2. Density and refractive index

Densities and refractive indexes of NdF_3–Al_2O_3–SiO_2, NdF_3–AlF_3–GeO_2, NdF_3–BaF_2–GeO_2, TbF_3–BaF_2–AlF_3–GeO_2, HoF_3–BaF_2–AlF_3–GeO_2, and $10LnF_3$–$20BaF_2$–$10AlF_3$–$60GeO_2$ system glasses are shown in Fig. 12. In Fig. 12, (−) and (+), respectively, correspond to data of typical oxide and fluoride glasses taken from the database, ''INTERGLAD'' [9]. The oxide glasses in this case include quartz glass [10], borosilicate glass (COVER 18–18; Iwaki Glass Co. Ltd.), PbO–WO_3–P_2O_5–CdO–TiO_2 glass [11], and various oxide glasses in the literature found in the INTERGLAD database [9]. In addition, ZBLAN [12–17] glass and others found in the database were chosen as fluoride glasses. Curves (A and B) in Fig. 12 were derived, respectively, by fitting the equation ($n = C_1 \exp(C_2 d)$ where C_1 and C_2 are constants) to data of oxide glasses and fluoride glasses. These empirical curves emphasize characteristics of the oxide and the fluoride glasses. Plots of the oxide fluoride glasses are located between curves (A and B). Especially, TbF_3–BaF_2–$10AlF_3$–GeO_2, HoF_3–BaF_2–$10AlF_3$–GeO_2, LnF_3–BaF_2–$10AlF_3$–GeO_2 (Ln; Y–Nd, Sm–Lu) glasses prepared in this study had a constant refractive index regardless of their respective densities. The relationship between density and refractive index is generally given by the Lorentz–Lorenz equation, as following [11]:

$$\frac{n^2-1}{n^2+2}V = \frac{4\pi N\alpha}{3} = R_L \quad (1)$$

Therein, n, V, N, α and R_L, respectively, represent the refractive index, molecular volume, Avogadro's number, polarizability, and molecular refraction. The Gladstone–Dale equation is

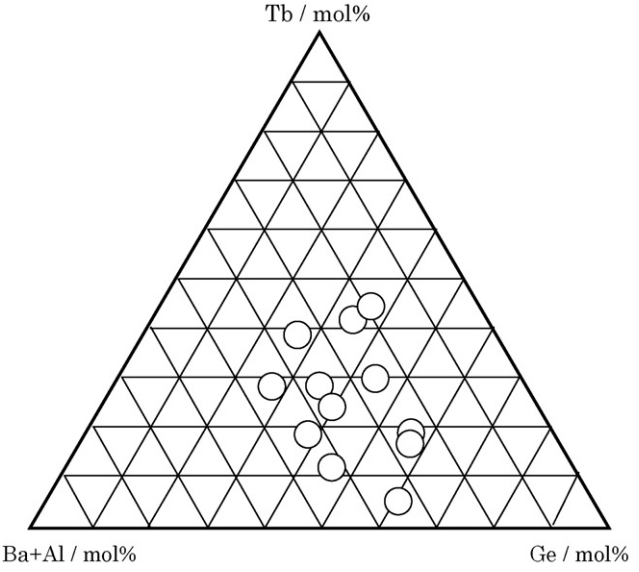

Fig. 11. Cationic composition in the glass of TbF_3–BaF_2–$10AlF_3$–GeO_2 system measured by EPMA.

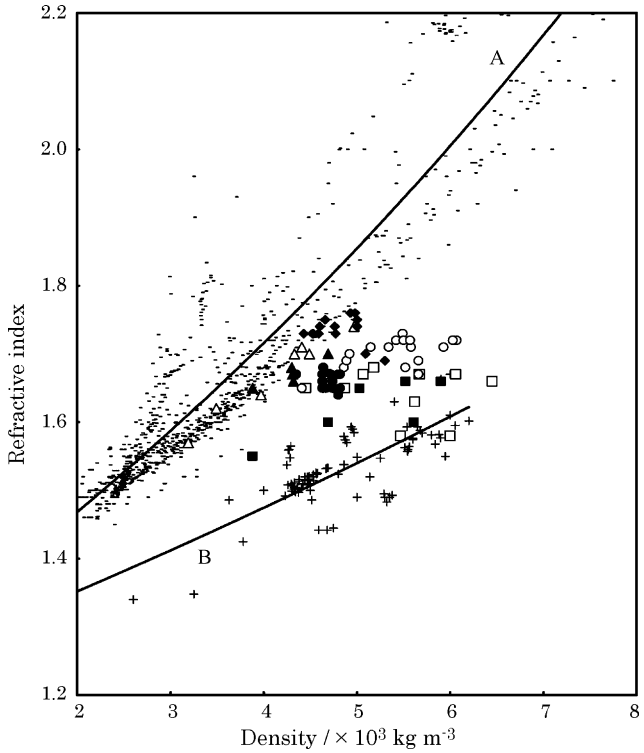

Fig. 12. Relationship between density and the refractive index for various glasses. (−) oxide glass*; (+) fluoride glass*; (▲) NdF_3–Al_2O_3–SiO_2; (△) NdF_3–AlF_3–GeO_2; (◆) NdF_3–BaF_2–GeO_2; (●) LnF_3–BaF_2–AlF_3–GeO_2 (Ln; Y–Nd, Sm–Lu); (○) TbF_3–BaF_2–AlF_3–GeO_2; (■) HoF_3–BaF_2–AlF_3–GeO_2; (□) TbF_3–BaF_2–AlF_3–SiO_2 (*data from INTERGRAD [14]).

Table 1
Glass transition temperatures of HoF_3–BaF_2–AlF_3–GeO_2 glasses

HoF_3:BaF_2:AlF_3:GeO_2	T_g (°C)
10:10:10:70	592.0
20:10:10:60	599.8
30:10:10:50	614.4
40:10:10:40	608.3
50:10:10:30	572.3
10:20:10:60	599.9
20:20:10:50	600.9
30:20:10:40	585.7
40:20:10:30	564.5
50:20:10:20	541.8
10:30:10:50	576.8
20:30:10:40	561.9

derived from Eq. (1) when n is close to 1, as the following [11]:

$$n - 1 = \frac{R}{V} = \frac{2\pi N\alpha}{V} = \frac{2\pi N\alpha}{M} d = R_G d \quad (2)$$

In those equations, M, d and R_G, respectively, denote the molecular weight, density and the Gladstone–Dale constant. Generally, this equation is used to express the relationship between density and the refractive index of a glass. The R_G value varies with glass composition. The R_G of the fluoride, the oxide and the oxide fluoride glasses were 0.9×10^{-4} to 1.4×10^{-4}, 1.8×10^{-4} to 2.9×10^{-4}, and 1.0×10^{-4} to 1.8×10^{-4}, respectively. Data of the NdF_3–Al_2O_3–SiO_2 system closely approximated the curve (A) corresponding to oxide glasses in Fig. 12. The glass network of NdF_3–Al_2O_3–SiO_2 was suggested to be an oxide such as Al_2O_3 and SiO_2. However, in the case of NdF_3–AlF_3–GeO_2 or NdF_3–BaF_2–GeO_2, systems in which the glass matrix consists of both an oxide and a fluoride, the plots of the refractive index against the density deviated from curve (A) to curve (B), corresponding to that of the fluoride glasses in Fig. 2. In the case of LnF_3–BaF_2–AlF_3–GeO_2 glasses, the plots were located between curves (A and B).

Table 2
Glass transition temperatures of TbF_3–BaF_2–AlF_3–GeO_2 glasses

TbF_3:BaF_2:AlF_3:GeO_2	T_g (°C)
10:10:10:70	606.7
20:10:10:60	631.1
30:10:10:50	619.9
40:10:10:40	628.8
50:10:10:30	618.2
10:20:10:60	578.4
20:20:10:50	603.4
30:20:10:40	593.4
40:20:10:30	574.0
10:30:10:50	593.0
20:30:10:40	583.4
30:30:10:30	571.9
30:0:10:60	675.2
40:0:10:50	669.1
50:0:10:40	639.9
30:0:20:50	664
40:0:20:40	610.8
30:0:30:40	605.1
40:0:30:30	622.2

Table 3
Glass transition temperatures of TbF_3–BaF_2–AlF_3–SiO_2 glasses

TbF_3–BaF_2–AlF_3–SiO_2	T_g (°C)
30:10:10:50	666.5
40:10:10:40	633.1
50:10:10:30	590.0
10:20:10:60	657.6
20:20:10:60	608.3
30:20:10:40	588.7

Data of glasses that consisted of 70 mol% oxide and 30 mol% fluoride ($10HoF_3$–$10BaF_2$–$10AlF_3$–$70GeO_2$) closely approximated curve (A) for oxide glasses. Data of glasses consisting of 30 mol% oxide and 70 mol% fluoride ($50HoF_3$–$10BaF_2$–$10AlF_3$–$30GeO_2$) closely approximated curve (B) for the fluoride glass area. Consequently, the oxide fluoride glasses were located at the intermediate area in the relationship between the refractive index and the density. No data for the simple oxide or fluoride glass was reported in this region previously.

2.1.3. Glass transition temperature

Respective glass transition temperatures of the HoF_3–BaF_2–$10AlF_3$–GeO_2 glasses, TbF_3–BaF_2–AlF_3–GeO_2 glasses, TbF_3–BaF_2–$10AlF_3$–SiO_2 glasses and $10LnF_3$–$20BaF_2$–$10AlF_3$–$60GeO_2$ glasses are listed in Tables 1–4. The glass transition temperatures of BaF_2-free glasses were higher than those of quaternary systems such as LnF_3–BaF_2–AlF_3–GeO_2 glasses. Glasses containing a larger amount of BaF_2 as a network modifier tend to have lower glass transition temperatures because divalent ions such as Ba^{2+} cut the glass network. Fluoride glasses like ZBLAN [12–17] exhibit a glass transition temperature around 300–400 °C. Oxide fluoride glasses obtained in this study must be more thermally stable than the fluoride glasses.

2.2. Optical properties of HoF_3–BaF_2–AlF_3–GeO_2 glasses

Some studies have explored oxide fluoride, oxyfluoride and fluorophosphate glasses [18–24]. Oxide fluoride glasses have

Table 4
Glass transition temperatures of LnF_3–BaF_2–AlF_3–GeO_2 (Ln; Y–Nd, Sm–Lu) glasses

Composition	T_g (°C)
$10YF_3$–$20BaF_2$–$10AlF_3$–$60GeO_2$	608.4
$10LaF_3$–$10BaF_2$–$10AlF_3$–$70GeO_2$	630.3
$10CeF_3$–$20BaF_2$–$10AlF_3$–$60GeO_2$	585.3
$10PrF_3$–$20BaF_2$–$10AlF_3$–$60GeO_2$	582.2
$10NdF_3$–$20BaF_2$–$10AlF_3$–$60GeO_2$	590.1
$10SmF_3$–$20BaF_2$–$10AlF_3$–$60GeO_2$	589.6
$10EuF_3$–$20BaF_2$–$10AlF_3$–$60GeO_2$	586.7
$10GdF_3$–$20BaF_2$–$10AlF_3$–$60GeO_2$	592.8
$10TbF_3$–$20BaF_2$–$10AlF_3$–$60GeO_2$	578.4
$10DyF_3$–$20BaF_2$–$10AlF_3$–$60GeO_2$	599.3
$10HoF_3$–$20BaF_2$–$10AlF_3$–$60GeO_2$	599.9
$10ErF_3$–$20BaF_2$–$10AlF_3$–$60GeO_2$	609.8
$10TmF_3$–$20BaF_2$–$10AlF_3$–$60GeO_2$	579.5
$10YbF_3$–$20BaF_2$–$10AlF_3$–$60GeO_2$	583.4
$10LuF_3$–$20BaF_2$–$10AlF_3$–$60GeO_2$	581.0

been researched as host materials for optically active ions because they have comparatively low phonon energies that correspond to oxide glasses, and high chemical and mechanical stabilities related to fluoride glasses. Although oxide and fluoride ions have similar ionic radii, the ratio of oxide and fluoride ions in the glass must alter the coordination structure that affects the elements' functionality because of their different valences. For example, binary rare earth metal oxide fluorides such as $Nd_2Eu_2O_3F_6$ have an ordered ionic configuration that engenders higher electric conductivity than that of YSZ-11 [25]. Oxide fluoride materials containing multi cation species can exhibit unique properties because of their ordered/disordered ionic configuration. In this section, the optical properties related to contents of LnF_3 were reviewed by using HoF_3 as a probe.

From the results of the absorption spectra measurements in the ultraviolet–visible region, the HoF_3 contents affected the peak pattern. In that case, Judd–Ofelt theory [26] with the results of the absorption spectra and the refractive indices measurements can be useful to get the information about the glass structure. Some reports have described dependence of the spectra on the glass matrix species using calculation of Judd–Ofelt intensity parameters (Ω_λ parameters) for Ho^{3+} in different host lattices [8,19,27–34]. The refractive indices were measured at 488, 540 and 641 nm to calculate Ω_λ parameters. They were used to determine the relation between the refractive index ($n(\lambda)$) and the wavelength (λ) by least squares fitting to the Sellmeier's dispersion equation [34]:

$$n^2(\lambda) = 1 + \frac{S\lambda^2}{\lambda^2 - \lambda_0^2} \tag{3}$$

Therein, S and λ_0 are constants. The respective values of S and λ_0 obtained for $10HoF_3$–$20BaF_2$–$10AlF_3$–$60GeO_2$ glass were 300 and 1.14. Using Eq. (3), the refractive index was recalculated at the specific wavelength. On the other hand, no dependence of the refractive index on the wavelength was observed under the condition in this study for $50HoF_3$–$20BaF_2$–$10AlF_3$–$20GeO_2$ glass; therefore, $n(\lambda)$ was assumed to be constant, 1.57 herein. According to the method described in some Refs. [8,19,26–31,35–38], the experimental oscillator strengths, f_{exp}, of the $aJ \rightarrow bJ'$ transition at the transition mean wavelength λ are summarized in Tables 5 and 6.

Table 5
Measured and calculated oscillator strength for Ho^{3+} ions in $10HoF_3$–$20BaF_2$–$10AlF_3$–$60GeO_2$ glass

$^5I_8\rightarrow$	Wavelength (nm)	Oscillator strength, f ($\times10^{-6}$)		Δf ($\times10^{-6}$)
		f_{exp}	f_{cal}	
$^5F_5$	645.9	1.78	1.81	−0.030
$^5S_2$	542.6	0.388	0.634	−0.246
$^5F_4$	539.0	2.03	1.79	0.240
$^5F_3$	485.1	0.534	0.752	−0.218
$^5F_2$	474.6	0.438	0.300	0.138
$^3K_8$	468.4	0.504	0.526	−0.022
$^5G_5$	417.8	0.947	1.67	−0.723
$^5G_4$	384.4	0.587	0.187	0.400
$^3K_7$	379.3	0.282	0.0855	0.197

Table 6
Measured and calculated oscillator strength for Ho^{3+} ions in $50HoF_3$–$20BaF_2$–$10AlF_3$–$20GeO_2$ glass

$^5I_8\rightarrow$	Wavelength (nm)	Oscillator strength, f ($\times10^{-6}$)		Δf ($\times10^{-6}$)
		f_{exp}	f_{cal}	
$^5F_5$	645.9	0.300	0.278	0.022
$^5S_2$	542.6	0.117	0.0494	0.068
$^5F_4$	539.0	0.190	0.276	−0.086
$^5F_3$	485.1	0.125	0.0602	−0.065
$^5F_2$	474.6	0.0782	0.0478	−0.030
$^3K_8$	468.4	0.0275	0.0331	0.006
$^5G_5$	417.8	0.189	0.0869	−0.102
$^5G_4$	385.4	0.0151	0.0411	0.026
$^3K_7$	382.3	0.0366	0.00861	−0.028
$^3F_2$	357.5	0.258	0.00136	−0.257
$^3F_4$	334.3	0.0635	0.00323	−0.060

From these values, the intensity parameters in Judd–Ofelt theory were obtained as $\Omega_2 = 1.96 \times 10^{-20}$, $\Omega_4 = 0.64 \times 10^{-20}$, and $\Omega_6 = 0.11 \times 10^{-20}\,cm^2$ for $10HoF_3$–$20BaF_2$–$10AlF_3$–$60GeO_2$ glasses and $\Omega_2 = 0.05 \times 10^{-20}$, $\Omega_4 = 0.10 \times 10^{-20}$ and $\Omega_6 = 0.02 \times 10^{-20}\,cm^2$ for $50HoF_3$–$20BaF_2$–$10AlF_3$–$20GeO_2$ glasses. The calculated oscillator strength, f_{cal}, is also summarized in that table. The respective rms deviations of f_{exp} and f_{cal} were $\delta = 3.9 \times 10^{-7}$ and 1.1×10^{-7} for $10HoF_3$–$20BaF_2$–$10AlF_3$–$60GeO_2$ and $50HoF_3$–$20BaF_2$–$10AlF_3$–$20GeO_2$ glasses. Some empirical correlations of the intensity parameter and the local structure of the lanthanide ions have been stated in the literature [8,19,26–31]. In general, Ω_2 increases with the asymmetry of the local structure and the degree of covalency of the lanthanide–ligand bonds, whereas Ω_6 decreases with the degree of covalency. For glass matrices prepared in this study, no clear conclusions are discernible from Ω_λ parameters because of their large uncertainty, especially for Ω_2, but the small value of Ω_2 together with very small Ω_6 for our glasses compared to that for $LaAlO_3$ crystal containing Ho^{3+} [38] were inferred to result from the lower covalency of the holmium–ligand bonds: the environment around Ho^{3+} in the glasses prepared in this study could be strongly ionic. This tendency seems to be more particularly true for $50HoF_3$–$20BaF_2$–$10AlF_3$–$20GeO_2$ glasses than for $10HoF_3$–$20BaF_2$–$10AlF_3$–$60GeO_2$ glass. The ratios of Ω_2/Ω_6 were, respectively, 20 and 2.5 for $10HoF_3$–$20BaF_2$–$10AlF_3$–$60GeO_2$ and $50HoF_3$–$20BaF_2$–$10AlF_3$–$20GeO_2$ glasses. These ratios imply that the local structure in the $50HoF_3$–$20BaF_2$–$10AlF_3$–$20GeO_2$ glasses seems to be more symmetric than that in $10HoF_3$–$20BaF_2$–$10AlF_3$–$60GeO_2$ glass. This fact seems to be reflected on the change in the intensity ratio in fluorescence spectra with the Ho^{3+} content and be able to be applied to control the optical properties of this glass system.

2.3. Optical properties of co-doped with TbF_3 and SmF_3

It has been reported that some rare earth co-doped systems exhibit the enchantment of intensity of fluorescence [39–41]. Oxide fluoride glasses which can contain rare earth fluorides of more than 50 mol% have been reported above [42,43]. It is

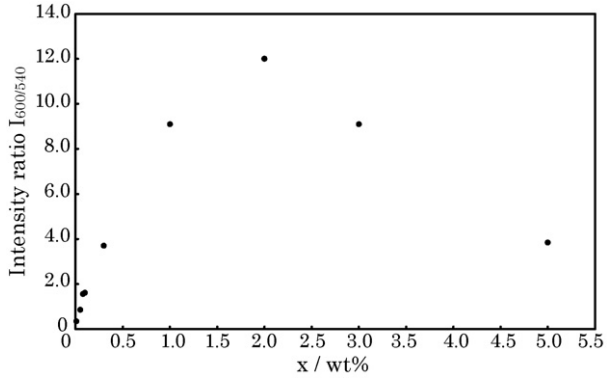

Fig. 13. Relationship between the intensity ratio ($I_{540/600}$) and contents of SmF_3 in $20TbF_3$–$20BaF_2$–$10AlF_3$–$50GeO_2$ mol%$^{-1}$ + x wt%$^{-1}$ SmF_3 glasses.

interesting to study the emission properties of such glasses in which two rare earth ions located very closely. In this section, some unique optical properties of the glass containing large amount of TbF_3 doped with very small amount of SmF_3 were mentioned.

Fig. 13 shows the relationship between $I_{600/540}$ (the ratio of the peak intensity at 540 nm originated from Tb^{3+} to that at 600 nm originated from Sm^{3+}) and the contents of SmF_3. $I_{600/540}$ increased with increasing content of SmF_3 (<2 wt%), whereas $I_{600/540}$ decreased with the contents of SmF_3 (>2 wt%). Some reports have revealed that concentration quenching of Sm^{3+} fluorescence occurred around 1–2 mol% [44,45]. It seems that the concentration quenching of Sm^{3+} fluorescence occurs when the content of SmF_3 is more than 2 wt% in Fig. 13. The intensities of fluorescence at 600 nm of Sm^{3+} in $20TbF_3$–$20BaF_2$–$10AlF_3$–$50GeO_2$ mol%$^{-1}$ + 2 wt% SmF_3 was measured as 1.2×10^4 cps while that in $20TbF_3$–$20BaF_2$–$10AlF_3$–$50GeO_2$ mol%$^{-1}$ + 5 wt% SmF_3 was 5.3×10^3 cps. This fact indicates that Sm^{3+} is dispersed identically in the $20TbF_3$–$20BaF_2$–$10AlF_3$–$50GeO_2$ glass without a phase-separated or otherwise clustered situation.

Fig. 14 shows the relationship between $I_{540/600}$ and the contents of TbF_3. Results showed that $I_{540/600}$ was proportional to $x^{2.05}$ by least-squares fitting where x was in $x TbF_3$–$20BaF_2$–$10AlF_3$–$(70 - x)GeO_2$ (mol%). The distance of Tb^{3+}–Tb^{3+} in the glass (D) is inversely proportional to the third power of the Tb^{3+} concentration, so $I_{540/600}$ is almost perfectly inversely proportional to the sixth power of D in this case. The theoretical calculation of Forster–Dexter [46,47] indicated that the resonant energy transfer probability is inversely proportional to the sixth power of the distance between two centers if the two centers belong to a dipolar transition. Therefore, the change in the relationship between $I_{540/600}$ and the contents of TbF_3 shown in Fig. 14 are explainable mainly using the concentration quenching of the Tb^{3+} fluorescence [48]. The TbF_3 content must be more than 20 mol% to obtain a glass that exhibits an intense orange emission. This phenomenon is a unique property for this LnF_3–BaF_2–AlF_3–GeO_2 system that can contain TbF_3 more than 50 mol%.

The fluorescence of $20TbF_3$–$20BaF_2$–$10AlF_3$–$50GeO_2$ + 0.05 wt% SmF_3 glass exhibited temperature dependence. The intensities of the peak at 540 nm originated from Tb^{3+} and the peak at 600 nm that originated from Sm^{3+} are mutually equivalent at room temperature. After heating to 573 K or cooling to 77 K, the intensity of the fluorescence that originated from Sm^{3+} decreased. The emission color changed from orange to green through yellow. The glass phase was stable at temperatures of 77–573 K because 673 K is much less than the glass transition temperature (876 K) of $20TbF_3$–$20BaF_2$–$10AlF_3$–$50GeO_2$ + 0.05 wt% SmF_3 glass. The emission color changed reversibly according to the temperature. Fig. 15 shows the relationship between the intensity ratio of $I_{600/540}$ and temperature. The change in the emission color from orange to green was recognized when $I_{600/540}$ was less than 0.7: $I_{600/540}$ decreased gradually by heating to 673 K. That emission color changed from orange to green through yellow. In the case of cooling, $I_{600/540}$ changed drastically and the emission color changed to green around 77 K. Relating the fluorescence peak to the energy transition $J \rightarrow J'$, where J and J' correspond to initial and final states respectively, the electrons in the ground state are excited and the population of J' becomes higher with increasing temperature. Therefore, the electrons at J barely transfer to J'. The intensity of the emission was lowered. The Tb^{3+} has a larger energy gap between J and J' than Sm^{3+} does. Therefore, the temperature affected the emission from Tb^{3+} only slightly; no significant concentration quenching occurred

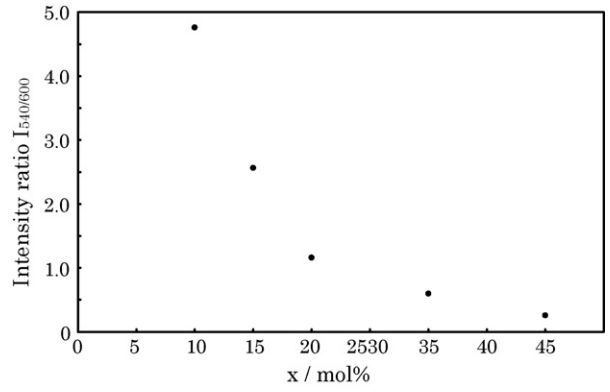

Fig. 14. Relationship between the intensity ratio ($I_{540/600}$) and contents of TbF_3 in $x TbF_3$–$20BaF_2$–$10AlF_3$–$(70 - x)GeO_2$ mol%$^{-1}$ + 0.05 wt%$^{-1}$ SmF_3 glasses.

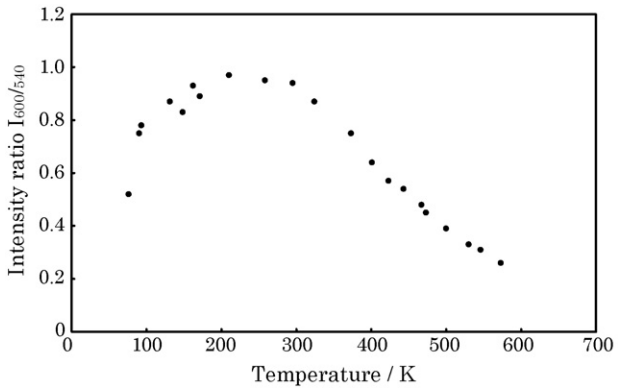

Fig. 15. Temperature dependence of the intensity ratio ($I_{600/540}$) of $20TbF_3$–$20BaF_2$–$10AlF_3$–$50GeO_2$ + 0.05 wt% SmF_3 glass.

in the case of Tb^{3+} [49]. Fig. 15 shows that, when the temperature rose, the emission from Tb^{3+} came to take precedence over Sm^{3+} for the system containing Tb^{3+} and Sm^{3+}. In the case of cooling, the mechanism is described as follows. Energy used for the emission from Sm^{3+} was supplied by non-radiative relaxation from Tb^{3+}. This non-radiative relaxation was called a multi-phonon relaxation, which was related to the lattice vibration and dipole–dipole interaction [50,51]. This multi-phonon relaxation occurred only slightly around 77 K. Therefore, the energy cannot be supplied from Tb^{3+} to Sm^{3+} when the sample temperature was lower than 77 K. As a result, the emission from Tb^{3+} was predominant and the emission color was green around 77 K. The reversible change in the emission color is a unique property of the LnF_3–BaF_2–AlF_3–GeO_2 glasses that have thermal stability. It is expected that these phenomena are useful to probe the energy transfer mechanism in the glass matrix.

2.4. Magnetic property of TbF_3 containing oxide fluoride glasses

Tb^{3+} is one of the rare earth ions having large effective magnetic moment, $9.72\mu_B$, which is the third among the rare earth ions. Considering the transparency of Tb^{3+} in the visible light region, Tb^{3+} containing compound is a very interesting to prepare a material for optical and magnetic applications [18,41,52,53]. Using TbF_3–BaF_2–AlF_3–GeO_2 system, the glass which contains a large amount of Tb^{3+} (50 mol% as TbF_3) could be prepared as mentioned above. Magnetic measurements were carried out at 77–273 K using a vibrating sample magnetometer (VSM) (Toei Industry Co. Ltd., VSM-3) with a maximum magnetic field of −10,000 to 10,000 Oe. Physical Properties Measurement System (PPMS) susceptometer (Quantumn Design Co.) is also used to investigate the relationship between magnetization and temperature at 2–300 K [54]. Fig. 16 shows the relationship between TbF_3 contents in $xTbF_3$–$20BaF_2$–$10AlF_3$–$(70-x)GeO_2$ mol%$^{-1}$ glass and magnetic susceptibility at room temperature. Generally, the relationship between magnetization and the magnetic field is shown as:

$$\vec{M} = \chi\vec{H} \tag{4}$$

where χ represents the magnetic susceptibility (emu mol^{-1}). The magnetic susceptibility is expressed as Eq. (5) from Curie–Weiss law:

$$\chi = \frac{C}{T-\theta} \tag{5}$$

θ is Weiss temperature and C is the Curie constant. C is written as

$$C = \frac{ng^2\mu_B^2 J(J+1)}{3k_B} = \frac{nM_{eff}^2}{3k_B} \tag{6}$$

where n, g, μ_B, k_B, J, and M_{eff}, respectively, represent the number of magnetic ions per mol, the Landé g-factor, Bohr magneton, total angular momentum, and the effective magnetic moment. The solid line in Fig. 16 was calculated from Eqs. (4)–(6). The magnetic susceptibilities are proportional to the contents of TbF_3 in the glasses obtained in this study. Their values fit the calculated values. Fig. 17 shows the magnetic susceptibility and the reciprocal magnetic susceptibility (χ^{-1}) of $30TbF_3$–$20BaF_2$–$10AlF_3$–$40GeO_2$ glass from 2 to 300 K. The relationship between χ^{-1} and temperature was linear as shown in Fig. 17. Weiss temperature which is an intersection point of χ^{-1} axis and temperature axis is almost zero. It means that the spin–spin interaction was negligible at 100–275 K in

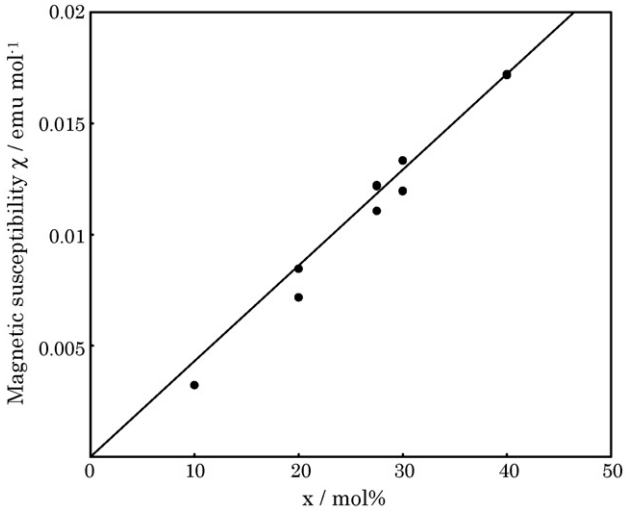

Fig. 16. The relationship between TbF_3 contents in the glass and magnetic susceptibility at room temperature. x is in $xTbF_3$–$20BaF_2$–$10AlF_3$–$(70-x)GeO_2$ (mol%). The solid line represents the theoretical relationship.

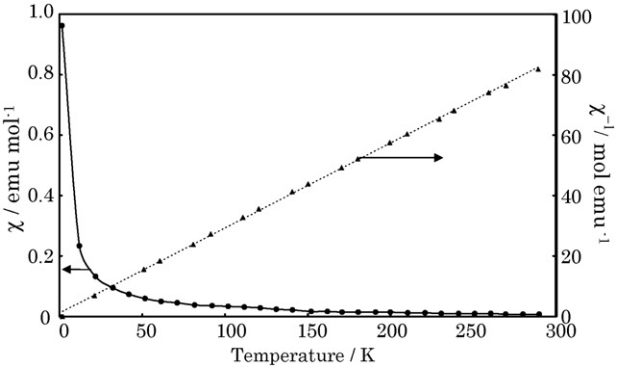

Fig. 17. Temperature dependence of magnetic susceptibility of $30TbF_3$–$20BaF_2$–$10AlF_3$–$40GeO_2$ glass.

Table 7
Curie constant and effective magnetic susceptibility of $xTbF_3$–$20BaF_2$–$10AlF_3$–$(70-x)GeO_2$ glasses (x = 10–40 mol%$^{-1}$)

Concentration of TbF_3 (mol%)	Curie constant (K)	Effective magnetic susceptibility, μ_B
10.0	1.00	8.83
20.0	2.47	9.77
27.5	3.12	9.37
30.0	4.49	10.7
40.0	5.13	9.96

the obtained glasses here. From the Eqs. (5) and (6), Curie constant (C) and the effective magnetic moment (M_{eff}) was calculated. These values were summarized in Table 7. The Curie constant increased with increasing glass TbF_3 contents. In addition, the effective magnetic susceptibility is consistent with the theoretical value, $9.78\mu_B$. Therefore it is obvious that the magnetic moment is derived only from a trivalent terbium ion. The atomic content of Tb^{3+} in $40TbF_3$–$20BaF_2$–$10AlF_3$–$30GeO_2$ was calculated as 11%, which is comparable to that reported for oxide glasses as the maximum one, 12% [55]. In addition, the saturation behavior might result from the $Tb^{3+}(\downarrow)$–O^{2-}–$Tb^{3+}(\uparrow)$ superexchange interaction, which prevented orientation of Tb^{3+} magnetic moments to the applied magnetic fields in the case of the oxide glasses [56]. Using fluoride instead of oxide is one way to restrain this saturation behavior. The atomic content of Tb^{3+} in $50TbF_3$–$20BaF_2$–$10AlF_3$–$20GeO_2$ glass obtained in this study was calculated as 14%. Therefore, it might have high potential for use as a material for Faraday devices [56].

References

[1] M. Takashima, S. Yonezawa, J.-H. Kim, J. Alloys Compd. 408–412 (2006) 468–473.
[2] T. Tamaoka, S. Tanabe, S. Ohara, H. Hayashi, N. Sugimoto, J. Alloys Compd. 408–412 (2006) 848–851.
[3] L.A. Bueno, et al. J. Non-Cryst. Solids 351 (2005) 1743–1746.
[4] S. Tanabe, T. Kouda, T. Hanada, J. Non-Cryst. Solids 274 (2000) 55–61.
[5] J.A. Medeiros-Neto, et al. J. Non-Cryst. Solids 184 (1995) 292–296.
[6] D. Raasch, H. Wierenga, J. Magn. Magn. Mater. 168 (1997) 336–346.
[7] S. Yonezawa, J.H. Kim, M. Takashim, Solid State Sci. 4 (2002) 1481–1485.
[8] M.R. Reddy, S.B. Raju, N. Veeraiah, J. Phys. Chem. Solids 61 (2000) 1567–1571.
[9] New Glass Forum INTERGLAND ver. 5 [on line database], 2004.
[10] R.B. Sosman, The Properties of Silica, Chemical Catalog, Reinhold, New York, 1927.
[11] T. Kano, H. Yanagida, Rare Earth—Properties and Applications, Gihodo Shuppan, Tokyo, 1990, p. 159.
[12] K. Soga, J. Kaga, H. Inoue, A. Makishima, J. Non-Cryst. Solids 315 (2003) 1–6.
[13] Y. Jestin, A. Le Sauze, B. Boulard, Y. Gao, P. Baniel, J. Non-Cryst. Solids 320 (2003) 231–237.
[14] A. Boutarfaia, M. Poulain, Solid State Ionics 144 (2001) 117–121.
[15] C.C. Chen, Y.J. Wu, L.G. Hwa, Mater. Chem. Phys. 65 (2000) 306–309.
[16] Y. Nishida, T. Kanamori, T. Sakamoto, Y. Ohishi, S. Sudo, J. Non-Cryst. Solids 221 (1997) 238–244.
[17] F. Gan, J. Non-Cryst. Solids 184 (1995) 9–20.
[18] K.K. Mahato, S.B. Rai, Spectrochim. Acta Part A 56 (2000) 2333–2340.
[19] S.B. Rai, Spectrochim. Acta Part A 58 (2002) 1559–1566.
[20] L.F. Santos, R.M. Almeida, V.K. Tikhomirov, A. Jha, J. Non-Cryst. Solids 284 (2001) 43–48.
[21] R. El-Mallawany, A.H. Khafagy, M.A. Ewaida, I.Z. Hager, M.A. Poulain, M.J. Poulain, J. Non-Cryst. Solids 184 (1995) 141–146.
[22] R.R. Reddy, Y.N. Ahammed, P.A. Azeem, K.R. Gopal, T.V.R. Rao, S. Buddhudu, N.S. Hussain, J. Quantitative Spectrosc. Radiative Transfer 77 (2003) 149–163.
[23] L.R. Moorthy, T.S. Rao, K. Janardhanam, A. Radhapathy, J. Alloys Compd. 298 (2000) 59–67.
[24] Y. Zhanci, H. Shihua, L. Shaozhe, C. Baojiu, J. Non-Cryst. Solids 343 (2004) 154–158.
[25] M. Takashima, S. Yonezawa, Y. Ukuma, J. Fluorine Chem. 87 (1998) 229–234.
[26] B.R. Judd, Phys. Rev. 127 (1962) 750–761.
[27] E. Rukmini, C.K. Jayasankar, Opt. Mater. 4 (1995) 529–546.
[28] S.B. Rai, A.K. Singh, S.K. Singh, Spectrochim. Acta Part A 59 (2003) 3221–3226.
[29] K. Driesen, C. Gorller-Walrand, K. Binnemans, Mater. Sci. Eng. C 18 (2001) 255–258.
[30] M. Malinowski, A. Wnuk, Z. Frukacz, G. Chadeyaron, R. Mahiou, S. Guy, M.F. Joubert, J. Alloys Compd. 323–324 (2001) 731–735.
[31] P.J. Deren, J.-C. Krupa, J. Alloys Compd. 380 (2004) 362–367.
[32] A. Lorenzo, L.E. Bausa, J.A. Sanz-Garcia, J. Garcia-Sole, J. Phys. Condens. Matter 8 (1996) 5781–5791.
[33] G.S. Ofelt, J. Chem. Phys. 37 (1962) 511–520.
[34] M.A. Khashan, A.Y. Nassif, Opt. Commun. 198 (2001) 247–256.
[35] R.T. Genova, I.R. Martin, et al. J. Alloys Compd. 380 (2004) 167–172.
[36] X. Qiao, X. Fan, M. Wang, X. Zhang, Opt. Matter 27 (2004) 597–603.
[37] W.T. Carnall, P.R. Fields, K. Rajnak, J. Chem. Phys. 49 (1968) 4424–4442.
[38] C. Gorller-Walrand, K. Binnemans, Handbook on the Physics and Chemistry of Rare Earths, vol. 25, 1998, p. 101 (and references therein).
[39] Y. Yang, S. Zhang, Q. Su, Mater. Res. Bull. 40 (2005) 1010–1017.
[40] H. Lin, E.Y. Pun, X. Wang, X. Liu, J. Alloys Compd. 390 (2005) 197–201.
[41] X. Zou, H. Toratani, J. Non-Cryst. Solids 195 (1996) 113–124.
[42] M. Takashima, S. Yonezawa, T. Tokuno, H. Umehara, T. Kato, J. Fluorine Chem. 112 (2001) 241–246.
[43] S. Nishibu, S. Yonezawa, M. Takashima, J. Non-Cryst. Solids 351 (2005) 1239–1245.
[44] Y. Zhou, J. Lin, S. Wang, J. Solid State Chem. 171 (2003) 391–395.
[45] E. Malchukova, B. Boizot, D. Ghaleb, G. Petite, Nucl. Instrum. Methods Phys. Res. Sect. A 537 (2005) 411–414.
[46] R.M. Clegg, Curr. Opin. Biotechnol. 6 (1995) 103–110.
[47] G.A. Kunar, N.V. Unnikrishnan, J. Photochem. Photobiol. A 144 (2001) 107–117.
[48] M. Nikl, N. Solovieva, M. Dusek, A. Yoshikawa, Y. Kagamitani, T. Fukuda, J. Ceram. Proc. Res. 4 (2003) 112–114.
[49] L.A. Riseberg, H.W. Moos, Phys. Rev. 174 (1968) 429–438.
[50] K.K. Mahato, D.K. Rai, S.B. Rai, Solid State Commun. 108 (1998) 671–676.
[51] D.J. Robbins, B. Cockayne, B. Lent, J.L. Glasper, Solid State Commun. 20 (1976) 673–676.
[52] D. Kaczorowski, K. Gofryk, L. Romaka, Ya. Mudryk, M. Konyk, P. Rogl, Intermetallics 13 (2005) 484–489.
[53] Y. Isikawa, D. Kato, A. Mitsuda, T. Mizushima, T. Kuwai, J. Magn. Magn. Mater. 272 (2004) 635–636.
[54] S. Nishibu, T. Nishio, S. Yonezawa, J.H. Kim, M. Takashima, H. Kikuchi, H. Yamamoto, J. Fluorine Chem. 127 (2006) 821–823.
[55] T. Hayakawa, M. Nogami, N. Nishi, N. Sawanobori, Chem. Mater. 14 (2002) 3223–3225.
[56] D. Imaizumi, T. Hayakawa, M. Nogami, J. Lightwave Technol. 20 (2002) 740–744.